Hindawi Publishing Corporation
Journal of Nanomaterials
Volume 2015, Article ID 896185, 6 pages
http://dx.doi.org/10.1155/2015/896185

Research Article

Laser-Assisted Synthesis of $Mn_{0.50}Zn_{0.50}Fe_2O_4$ Nanomaterial: Characterization and *In Vitro* Inhibition Activity towards *Bacillus subtilis* Biofilm

Shaukat Ali Shahid,[1] Farooq Anwar,[2,3] Muhammad Shahid,[4] Nazia Majeed,[4] Ahmed Azam,[1] Mamoona Bashir,[1] Muhammad Amin,[2] Zahed Mahmood,[5] and Imran Shakir[6]

[1]*Department of Physics, University of Agriculture, Faisalabad 38040, Pakistan*
[2]*Department of Chemistry, University of Sargodha, Sargodha 40100, Pakistan*
[3]*Department of Pharmaceutical Chemistry, College of Pharmacy, Prince Sattam bin Abdulaziz University, P.O. Box 173, Al-Kharj 11942, Saudi Arabia*
[4]*Department of Biochemistry, University of Agriculture, Faisalabad 38040, Pakistan*
[5]*Department of Applied Chemistry & Biochemistry, Government College University, Faisalabad 38000, Pakistan*
[6]*Deanship of Scientific Research College of Engineering, King Saud University, P.O. Box 800, Riyadh, Saudi Arabia*

Correspondence should be addressed to Shaukat Ali Shahid; shaukatshahid92@gmail.com

Received 19 November 2014; Accepted 16 February 2015

Academic Editor: Ali Khorsand Zak

There is growing interest in the development of novel nanomaterials with potential antimicrobial activity and lesser toxicity. In the current research work, $Mn_{0.5}Zn_{0.5}Fe_2O_4$ nanoparticles were synthesized via a novel coprecipitation cum laser ablation technique yielding fine spinal structured material. The synthesized nanomaterial was structurally characterized by X-ray diffraction technique which confirmed the formation and the crystalline nature of $Mn_{0.50}Zn_{0.50}Fe_2O_4$ nanomaterial. The crystallite size determined by Debye-Scherrer's formula was found to be ~12 nm. The formation of nanoparticles was evidenced by scanning electron microscopy. Energy dispersive X-ray analysis (EDXA) was performed for elemental analysis. The synthesized nanomaterial was interestingly found to be an effective antimicrobial agent and inhibited the growth of *Bacillus subtilis* biofilm formation. The 5 μg of $Mn_{0.5}Zn_{0.5}Fe_2O_4$ nanomaterial dissolved in 1 mL of DMSO showed excellent biofilm inhibitory activity 91.23% ± 1.87 against *Bacillus subtilis*.

1. Introduction

Preparation of nanosized fine spinal structure is an emerging research area in the field of nanotechnology. Presently, the applications of such nanomaterials are being explored to address the problems associated with water treatment, and so forth [1], catalysis [2], and microbial control [3, 4]. Nanosize metal particles can provide considerably large surface area as compared to bulk material. Theoretically, for spherical particles of identical size, a decrease in the particle size from 10 μm to 10 nm can escalate the contact surface area by 10^9 [5, 6].

Biofilms are aggregates of microorganisms formed by the attachment of microbial cells in polymeric substances [7]. Mostly, biofilms are highly resistant to antibiotics and are therefore being extensively studied in quite a lot of scientific disciplines, including evolutionary biology, biomedicine, and water treatment [8–11]. The growth of a microbial biofilm initiates with the attachment of free-floating microorganisms to a surface. Subsequently, these adherent microbes are entrenched repeatedly within a self-produced medium of extracellular polymeric substances (EPS) usually composed of extracellular DNA, proteins, and polysaccharides. These bacterial biofilms can cause several infectious diseases and develop resistance manifold [11–13].

In the recent past, use of metal-based nanoparticles for curing bacterial infections has got great scientific interest [14].

Some *in vitro* studies revealed that the metal nanoparticles exhibited potential antibiofilm activity as tested on biofilms formed by *Pseudomonas aeruginosa* and *Staphylococcus epidermidis* [14, 15]. The antibacterial efficiency of metal nanoparticles is not only due to metal-ion release but mostly based on their high surface-to-volume ratio [15].

Although coprecipitation is considered convenient method to prepare nanomaterials, it is rather difficult to prepare fine nanostructure with larger surface area using this approach. Therefore, we were motivated to prepare $Mn_{0.5}Zn_{0.5}Fe_2O_4$ by novel coprecipitation cum laser ablation technique with the expectation of improved performance for inhibition of *Bacillus subtilis* biofilm. Furthermore, to the best of author's knowledge, $Mn_{0.5}Zn_{0.5}Fe_2O_4$ has never been investigated by microtiter-plate assay for inhibition of *Bacillus subtilis* biofilm. To bridge the research gap in biofilm inhibition using novel $Mn_{0.5}Zn_{0.5}Fe_2O_4$ nanomaterial is fascinating task; hence, we report synthesis of $Mn_{0.5}Zn_{0.5}Fe_2O_4$ nanoparticles using coprecipitation approach followed by laser irradiation technique to assess their potential application in *Bacillus subtilis* biofilm inhibition by microtiter-plate assay [16].

2. Materials and Methods

2.1. Chemicals. All the chemicals ($MnCl_2{\cdot}4H_2O$, $ZnCl_2$, $FeCl_3{\cdot}6H_2O$, and NaOH) used in the synthesis were analytical reagent grade (99.9% purity) (purchased from Sigma Chemical Company Co., St. Louis, MO, USA) and were used without further purification.

2.2. Synthesis of $Mn_{0.5}Zn_{0.5}Fe_2O_4$ Nanoparticles. For the synthesis of $Mn_{0.5}Zn_{0.5}Fe_2O_4$ nanoparticles by chemical coprecipitation technique [1, 2], a 0.5 M solution of analytical grade $MnCl_2{\cdot}4H_2O$ and 0.5 M of $ZnCl_2$ were prepared by dissolving in 50 mL sterile deionized water. Another solution was prepared by dissolving 1 M of $FeCl_3{\cdot}6H_2O$ in 50 mL sterile deionized water. These stoichiometric quantities led to the formation of atomic ratios 1 : 1 : 4 for Mn : Zn : Fe in $Mn_{0.5}Zn_{0.5}Fe_2O_4$. These two solutions were homogenized by stirring at 65°C for 30 min using hot plate magnetic stirrer at moderate speed (55 rpm). For precipitation of chloride precursors, the solution pH was increased to 10 by adding dropwise 3.5 M NaOH with continuous stirring (it took about 120 min) until reddish brown precipitates formed. To get fine spinal structure of nanomaterial, thermal decomposition of Mn, Zn, and Fe chlorides was performed by irradiation of solution for 5 min with a 532 nm green laser beam (20 mW power) produced with Continuous Wave (CW) Diode Pumped Solid State Laser (DPSSL) Model CDPS532M-020 (JDS Uniphase Corp, USA). The synthesized material was then cooled to room temperature (30°C) and digested for 120 minutes to settle down the particles at the bottom of the beaker. The precipitate of $Mn_{0.5}Zn_{0.5}Fe_2O_4$ was filtered using Grade 287 filter paper (GE Healthcare Life Sciences) and then washed using deionized water till chloride became free and the pH of the residual solution reached 7.0. It took 6 to 7 hours to make the residual neutral. The recovered precipitates were dried for 90 min at 100°C in an oven and then ground with pestle and mortar into a fine powder followed by calcination at 700°C for 4 hours in a muffle furnace (Vulcan, A550).

2.3. Characterization of $Mn_{0.5}Zn_{0.5}Fe_2O_4$ Nanomaterial. The structural analysis of ultrafine homogeneous powder of $Mn_{0.5}Zn_{0.5}Fe_2O_4$ nanomaterial was performed using X-ray diffractometer (D8 FOCUS 2220 Bruker AXS) with Cu Kα radiation (λ = 1.5418 Å). The X-ray diffraction (XRD) pattern was recorded at a scanning rate of 0.02°/s in 2θ ranging from 10° to 80°. The gold coated specimen was utilized to appraise the morphologies of the nanoparticles by Scanning Electron Microscope (SEM, JEOL JSM 7401F JEOL Ltd., Akishima, Japan) operated at an accelerating voltage of 15 kV. The elemental analysis was performed by using energy dispersive X-ray microanalysis (EDX, Inca-FET-3, Oxford Instruments, UK Ltd.). The BET specific surface area was investigated by N_2 adsorption (77 K) using a Micromeritics ASAP 2000 system during the overnight treatment (130°C) under vacuum thereby degassing the sample. On average, BET specific surface area was found to be 78.3 $m^2\,g^{-1}$.

2.4. Assessment of Biofilm Inhibition. The inhibition of bacterial (*Bacillus subtilis*) biofilm formation was assessed by the microtiter-plate method as described by Stepanović et al. [16]. The wells of a sterile 24-well flat bottomed plastic tissue culture plate were filled with 100 μL of nutrient broth (Oxoid, UK). Two concentrations, that is, 2.5 and 5.0 μg of testing samples (dissolved in 1 mL of DMSO), were added in different wells. Finally, 20 μL of bacterial suspension containing 1×10^9 CFU/mL was inoculated. Positive control well contained Rifampicin and nutrient broth (Oxoid, UK) while negative control well contained nutrient broth and microbial strain. Afterwards, plates were covered and then incubated aerobically for 24 hours at 37°C. Thereafter, the contents of each well were behed thrice with 220 μL of sterile phosphate buffer (pH: 7.2). To remove all nonadherent bacteria, plates were vigorously shaken. Then, attached leftover bacteria were fixed with 220 mL of 99% methanol per well. Next, after 15 min, plates were emptied and left to dry. Then, plates were stained for 5 min with 220 mL of 50% crystal violet per well. Surplus stain was rinsed off using distilled water. Then plates were air-dried and the bound dye was resolubilized with 220 μL of 33% (v/v) glacial acetic acid per well. The optical density (OD) of each well was measured at 630 nm using microplate reader (Biotek, USA). All the tests were carried thrice against selected bacterial strain and the results were averaged. The bacterial growth inhibition (INH%) was calculated using the following formula:

$$\text{Inhibition}\,\% = 100 - \frac{\left(\text{OD}_{630\ \text{sample}} \times 100\right)}{\text{OD}_{630\ \text{control}}}. \quad (1)$$

3. Results and Discussion

3.1. Structural Analysis of $Mn_{0.5}Zn_{0.5}Fe_2O_4$ Nanomaterial. The powder X-ray diffraction patterns of $Mn_{0.5}Zn_{0.5}Fe_2O_4$ calcined at 700°C temperature exhibited sharp, intense

Table 1: Characterization data of XRD for $Mn_{0.5}Zn_{0.5}Fe_2O_4$.

Ferrite composition	$Mn_{0.5}Zn_{0.5}Fe_2O_4$
Lattice constant	8.583
Volume $(Å)^3$	632
Bulk density (gcm^{-3})	~4.00
X-ray density (gcm^{-3})	5.07
Pore volume (cm^3g^{-1})	0.27 ± 0.02
Crystallite size (nm)	~12

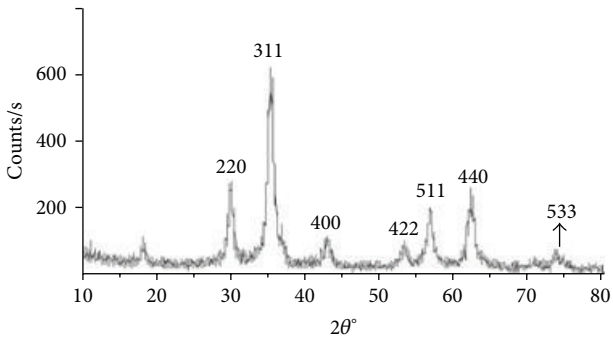

Figure 1: XRD pattern of $Mn_{0.5}Zn_{0.5}Fe_2O_4$.

diffraction peaks and single cubic phase with fcc structure of $Mn_{0.5}Zn_{0.5}Fe_2O_4$ without any impurity phase (Figure 1), revealing the highly crystalline character of the sample indexed with JCPDS card number 74-2401. The crystallite size determined by Debye-Scherrer's formula was found to be ~12 nm and the calculated lattice parameters α for $Mn_{0.5}Zn_{0.5}Fe_2O_4$ sample were found to be 0.869 nm (Table 1).

It is worth mentioning here that laser irradiation brings confined thermal modifications in the light absorbing structures; nevertheless it evades thermal destruction to the nearby structure due to its directionality. Besides, diode laser output is narrowband; hence most of it is absorbed and exploited during irradiation of the material producing the fine crystal structure.

The average particle size ~12 nm was estimated from ten particles at ×50,000 magnification from the SEM micrographs (Figure 2). Besides, it is evident from the SEM micrograph that $MnZnFe_2O_4$ sample has uniform and spherical structural morphology with a narrow size distribution of the particles.

For quantitative analysis, the as synthesized ultrafine homogeneous nanomaterial sample (in bulk, flat, and polished form) was exposed to electron beam of accelerating voltage 15 kV in electron microscope under high vacuum. The EDXA spectrum (Figure 3) of the $Mn_{0.5}Zn_{0.5}Fe_2O_4$ nanomaterial shows that it contains only Fe, Mn, Zn, and O with no traces of byproducts. Table 2 lists the relative abundance of each of the elements which is analogous to the theoretical stoichiometric values. No contamination is detected due to high purity of the starting materials used for the synthesis of the $Mn_{0.5}Zn_{0.5}Fe_2O_4$ nanoparticles.

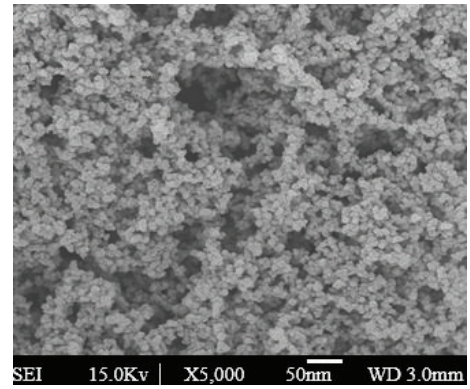

Figure 2: SEM micrograph of $Mn_{0.5}Zn_{0.5}Fe_2O_4$ nanoparticles.

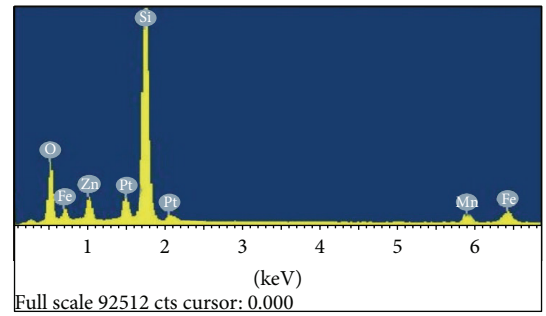

Figure 3: Energy dispersive X-ray spectra of $Mn_{0.5}Zn_{0.5}Fe_2O_4$.

Table 2: Characterization data of EDX for $Mn_{0.5}Zn_{0.5}Fe_2O_4$.

Elements	Weight %	Atomic weight %
O K	26.00	29.34
Mn K	9.21	5.23
Si K	38.68	37.11
Fe K	12.48	22.12
Zn L	10.57	5.36
Pt M	5.06	0.84
Total	100	

Table 3: *Bacillus subtilis* biofilm inhibition.

$Mn_{0.5}Zn_{0.5}Fe_2O_4$ nanoparticles dissolved in 1 mL of DMSO	Biofilm inhibition (%)
2.5 μg	88.44 ± 1.85
5.0 μg	91.23 ± 1.87
Rifampicin	98.12 ± 0.15

3.2. Bacillus subtilis Biofilm Inhibition Activity. Figure 4 depicted that 5 μg of $Mn_{0.5}Zn_{0.5}Fe_2O_4$ nanoparticles dissolved in 1 mL of DMSO showed excellent biofilm inhibitory activity 91.23% ± 1.87 against *Bacillus subtilis* (Table 3). This antibacterial potential of the tested nanomaterial can be attributed to the fact that the $Mn_{0.5}Zn_{0.5}Fe_2O_4$ nanoparticles have greater surface area and unique crystal form having

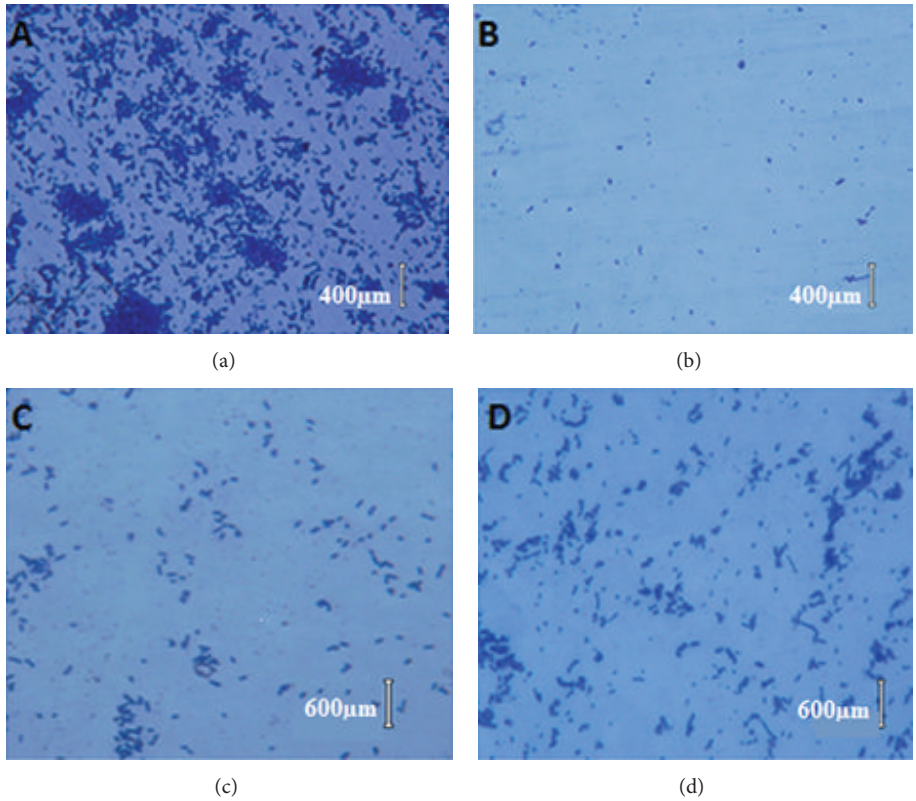

Figure 4: Phase contrast microscopic view of inhibition of *Bacillus subtilis* biofilm by $Mn_{0.5}Zn_{0.5}Fe_2O_4$ nanoparticles at 100x ((a) controlled (native) *Bacillus subtilis* biofilm; (b) Rifampicin treated control; (c) biofilm treated by 5.0 μg of $Mn_{0.5}Zn_{0.5}Fe_2O_4$ nanoparticles dissolved in 1 mL of DMSO; (d) biofilm treated by 2.5 μg of $Mn_{0.5}Zn_{0.5}Fe_2O_4$ nanoparticles dissolved in 1 mL of DMSO).

more sharp edges and site to enhance their activity by joining up with bacterial membrane to disrupt the membrane [14].

There may be different possible mechanisms of action for the observed antibacterial activity of $Mn_{0.5}Zn_{0.5}Fe_2O_4$ nanoparticles. For example, the tested nanoparticles stick to the bacterial cell wall and breach the cell membrane [17] and cause degradation and lysis of the cytoplasm, resulting in cell death. As nanoparticles possess large surface area, their bactericidal efficacy is enhanced contrary to the bulky particles with lesser surface area. Furthermore, the $Mn_{0.5}Zn_{0.5}Fe_2O_4$ nanoparticles keep a large surface-to-volume ratio, which leads to an increase in their bioactivity making them active and potent bactericidal agents [15, 18]. Previous studies on zinc nanoparticle structures revealed that zinc fixes to the membranes of microbes, analogous to mammalian cells by delaying their growth, thereby, prolonging the cell division time of the organism. Similarly, according to some other reports, the main chemical species linked to the antibacterial activity of such nanomaterials were supposed to be active oxides; for example, hydrogen peroxide (H_2O_2) formed from the surface of the ceramic zinc [19, 20]. Hydroxyl radicals are very strong oxidants and when nanoparticles directly stick to the microbes, their surface undergoes crucial oxidative attack. The active oxides eagerly penetrate through the bacterial cell wall and cause cell destruction and thus inhibit the bacterial growth [20, 21].

Typically, in the case of $Mn_{0.5}Zn_{0.5}Fe_2O_4$ nanoparticles, upon excitation by light, the photon energy produces a pair of electron and hole on the $Mn_{0.5}Zn_{0.5}Fe_2O_4$ surface. The hole (in the valence band) might have reacted with H_2O or hydroxide (OH) ions adsorbed on the surface producing hydroxyl radicals ($OH^\bullet$) while the electron (in the conduction band) reduces O_2 to generate superoxide ions (O_2^-). The holes and $OH^\bullet$ both are extremely reactive towards organic complexes [22, 23] and thus might have caused disruption of the cell membrane/cell wall of *Bacillus subtilis* and leakage of intracellular K^+ ions leading to cell death (Figures 4 and 5). Previously, outer cell membrane damage was noted by Sunada et al. [24] in case of *E. coli* wherein they found that the endotoxin, a vital part of the outer cell membrane, was smashed while photocatalysis was performed with TiO_2.

Polyunsaturated phospholipids are vital constituents of the bacterial cell membrane and high vulnerability of these organic compounds to be attacked by reactive oxygen species (ROS) is an established fact [25, 26]. Many functions, such as semipermeability, oxidative phosphorylation reactions, and respiration, are influenced by the cell membrane composition and structure. Therefore, lipid peroxidation is detrimental to all forms of life. Besides, the usual functionalities linked with an intact membrane, for example, respiratory activity, are vanished by lipid peroxidation reaction. Hence, any damage to bacterial cell membrane structure or modification

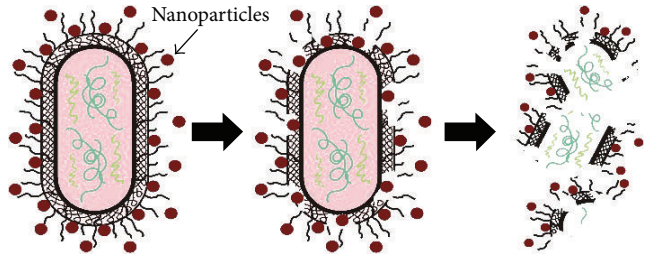

Figure 5: Mechanism of bactericidal action of $Mn_{0.5}Zn_{0.5}Fe_2O_4$ nanoparticles.

in membrane architecture and design initiated by lipid peroxidation causes alterations in membrane-bound proteins, electron mediators, orientation of compounds across the cell membrane, leakage of K^+ ions, and successive functional changes, thereby causing cell death upon contact with $Mn_{0.5}Zn_{0.5}Fe_2O_4$ nanoparticles [25, 26].

4. Conclusions

The bacterial biofilms can cause several infectious diseases and develop resistance against antibiotics. In the present study, for the first time, the antibacterial properties of $Mn_{0.5}Zn_{0.5}Fe_2O_4$ nanoparticles were established in an *in vitro* trial against biofilm formed by *Bacillus subtilis* using microtiter-plate assay. $Mn_{0.5}Zn_{0.5}Fe_2O_4$ nanoparticles showed excellent inhibitory effect against the highly multidrug-resistant Gram-positive bacterial strain *Bacillus subtilis*. The results indicate that the $Mn_{0.5}Zn_{0.5}Fe_2O_4$ nanocomposite is a promising disinfection material that can also be used in surface coatings to effectively inhibit bacterial growth and proliferation.

Conflict of Interests

The authors declare that there is no conflict of interests regarding the publication of this paper.

Acknowledgment

The authors would like to extend their sincere appreciation to the Deanship of Scientific Research at King Saud University for its funding of this research through the Research Group Project no. RGP-VPP-312.

References

[1] I. Ullah, S. Ali, M. A. Hanif, and S. A. Shahid, "Nanoscience for environmental remediation: a review," *International Journal of Chemical and Biochemical Sciences*, vol. 2, pp. 60–77, 2012.

[2] S. A. Shahid, A. Nafady, I. Ullah et al., "Characterization of newly synthesized $ZrFe_2O_5$ nanomaterial and investigations of its tremendous photocatalytic properties under visible light irradiation," *Journal of Nanomaterials*, vol. 2013, Article ID 517643, 6 pages, 2013.

[3] M. Raffi, S. Mehrwan, T. M. Bhatti et al., "Investigations into the antibacterial behavior of copper nanoparticles against *Escherichia coli*," *Annals of Microbiology*, vol. 60, no. 1, pp. 75–80, 2010.

[4] W.-L. Du, S.-S. Niu, Y.-L. Xu, Z.-R. Xu, and C.-L. Fan, "Antibacterial activity of chitosan tripolyphosphate nanoparticles loaded with various metal ions," *Carbohydrate Polymers*, vol. 75, no. 3, pp. 385–389, 2009.

[5] J. R. Morones, J. L. Elechiguerra, A. Camacho et al., "The bactericidal effect of silver nanoparticles," *Nanotechnology*, vol. 16, no. 10, pp. 2346–2353, 2005.

[6] C. Burda, X. Chen, R. Narayanan, and M. A. El-Sayed, "Chemistry and properties of nanocrystals of different shapes," *Chemical Reviews*, vol. 105, no. 4, pp. 1025–1102, 2005.

[7] J. S. Teodósio, M. Simões, L. F. Melo, and F. J. Mergulhão, "Flow cell hydrodynamics and their effects on *E. coli* biofilm formation under different nutrient conditions and turbulent flow," *Biofouling*, vol. 27, no. 1, pp. 1–11, 2011.

[8] S. Ganguly, S. K. Mukhopadhayay, and S. Biswas, "Potential threat to human health from foodborne illness having serious implications on public health—a review," *International Journal of Chemical and Biochemical Sciences*, vol. 1, pp. 65–68, 2012.

[9] J. W. Austin and G. Bergeron, "Development of bacterial biofilms in dairy processing lines," *Journal of Dairy Research*, vol. 62, no. 3, pp. 509–519, 1995.

[10] J. H. Carr, R. L. Anderson, and M. S. Favero, "Comparison of chemical dehydration and critical point drying for the stabilization and visualization of aging biofilm present on interior surfaces of PVC distribution pipe," *Journal of Applied Bacteriology*, vol. 80, no. 2, pp. 225–232, 1996.

[11] L. Hall-Stoodley, J. W. Costerton, and P. Stoodley, "Bacterial biofilms: from the natural environment to infectious diseases," *Nature Reviews Microbiology*, vol. 2, no. 2, pp. 95–108, 2004.

[12] G. Lear and G. D. Lewis, *Microbial Biofilms: Current Research and Applications*, Caister Academic Press, Norfolk, UK, 2012.

[13] E. Karatan and P. Watnick, "Signals, regulatory networks, and materials that build and break bacterial biofilms," *Microbiology and Molecular Biology Reviews*, vol. 73, no. 2, pp. 310–347, 2009.

[14] R. P. Allaker, "The use of nanoparticles to control oral biofilm formation," *Journal of Dental Research*, vol. 89, no. 11, pp. 1175–1186, 2010.

[15] P. K. Stoimenov, R. L. Klinger, G. L. Marchin, and K. J. Klabunde, "Metal oxide nanoparticles as bactericidal agents," *Langmuir*, vol. 18, no. 17, pp. 6679–6686, 2002.

[16] S. Stepanović, D. Vuković, I. Dakić, B. Savić, and M. Švabić-Vlahović, "A modified microtiter-plate test for quantification of staphylococcal biofilm formation," *Journal of Microbiological Methods*, vol. 40, no. 2, pp. 175–179, 2000.

[17] C.-H. Hu and M.-S. Xia, "Adsorption and antibacterial effect of copper-exchanged montmorillonite on *Escherichia coli* K88," *Applied Clay Science*, vol. 31, no. 3-4, pp. 180–184, 2006.

[18] O. Yamamoto and J. Sawai, "Preparation and characterization of novel activated carbons with antibacterial function," *Bulletin of the Chemical Society of Japan*, vol. 74, no. 9, pp. 1761–1765, 2001.

[19] J. Sawai, S. Shoji, H. Igarashi et al., "Hydrogen peroxide as an antibacterial factor in zinc oxide powder slurry," *Journal of Fermentation and Bioengineering*, vol. 86, no. 5, pp. 521–522, 1998.

[20] T. D. Wikins, L. V. Holdeman, I. J. Abramson, and W. E. Moore, "Standardized single-disc method for antibiotic susceptibility testing of anaerobic bacteria," *Antimicrobial Agents and Chemotherapy*, vol. 1, no. 6, pp. 451–459, 1972.

[21] A. E. Nel, L. Mädler, D. Velegol et al., "Understanding biophysicochemical interactions at the nano-bio interface," *Nature Materials*, vol. 8, no. 7, pp. 543–557, 2009.

[22] W. A. Jacoby, P. C. Maness, E. J. Wolfrum, D. M. Blake, and J. A. Fennell, "Mineralization of bacterial cell mass on a photocatalytic surface in air," *Environmental Science and Technology*, vol. 32, no. 17, pp. 2650–2653, 1998.

[23] O. Legrini, E. Oliveros, and A. M. Braun, "Photochemical processes for water treatment," *Chemical Reviews*, vol. 93, no. 2, pp. 671–698, 1993.

[24] K. Sunada, Y. Kikuchi, K. Hashimoto, and A. Fujishima, "Bactericidal and detoxification effects of TiO_2 thin film photocatalysts," *Environmental Science & Technology*, vol. 32, no. 5, pp. 726–728, 1998.

[25] P.-C. Maness, S. Smolinski, D. M. Blake, Z. Huang, E. J. Wolfrum, and W. A. Jacoby, "Bactericidal activity of photocatalytic TiO_2 reaction: toward an understanding of its killing mechanism," *Applied and Environmental Microbiology*, vol. 65, no. 9, pp. 4094–4098, 1999.

[26] T. Saito, T. Iwase, J. Horie, and T. Morioka, "Mode of photocatalytic bactericidal action of powdered semiconductor TiO_2 on mutans streptococci," *Journal of Photochemistry and Photobiology B: Biology*, vol. 14, no. 4, pp. 369–379, 1992.